Band offsets and trap-related electron transitions at interfaces of (100)InAs with atomic-layer deposited Al_2O_3

H.-Y. Chou, E. O'Connor, A. O'Mahony, I. M. Povey, P. K. Hurley, Lin Dong, P. D. Ye, V. V. Afanas'ev, M. Houssa, and A. Stesmans

Citation: J. Appl. Phys. **120**, 235701 (2016); doi: 10.1063/1.4971178
View online: http://dx.doi.org/10.1063/1.4971178
View Table of Contents: http://aip.scitation.org/toc/jap/120/23
Published by the American Institute of Physics

Band offsets and trap-related electron transitions at interfaces of (100)InAs with atomic-layer deposited Al_2O_3

H.-Y. Chou,[1] E. O'Connor,[2] A. O'Mahony,[2] I. M. Povey,[2] P. K. Hurley,[2] Lin Dong,[3] P. D. Ye,[3] V. V. Afanas'ev,[1] M. Houssa,[1] and A. Stesmans[1]
[1]*Laboratory of Semiconductor Physics, Department of Physics, University of Leuven, Leuven, Belgium*
[2]*Tyndall National Institute and Department of Chemistry, University College Cork, Lee Maltings, Prospect Row, Cork, Ireland*
[3]*School of Electrical and Computer Engineering and Birck Nanotechnology Center, Purdue University, West Lafayette, Indiana 47907, USA*

(Received 5 September 2016; accepted 17 November 2016; published online 15 December 2016)

Spectral analysis of optically excited currents in single-crystal (100)InAs/amorphous (a-)Al_2O_3/metal structures allows one to separate contributions stemming from the internal photoemission (IPE) of electrons into alumina and from the trapping-related displacement currents. IPE spectra suggest that the out-diffusion of In and, possibly, its incorporation in a-Al_2O_3 lead to the development of ≈0.4 eV wide conduction band (CB) tail states. The top of the InAs valence band is found at 3.45 ± 0.10 eV below the alumina CB bottom, i.e., at the same energy as at the GaAs/a-Al_2O_3 interface. This corresponds to the CB and the valence band offsets at the InAs/a-Al_2O_3 interface of 3.1 ± 0.1 eV and 2.5 ± 0.1 eV, respectively. However, atomic-layer deposition of alumina on InAs results in additional low-energy electron transitions with spectral thresholds in the range of 2.0–2.2 eV, which is close to the bandgap of AlAs. The latter suggests the interaction of As with Al, leading to an interlayer containing Al-As bonds providing a lower barrier for electron injection. *Published by AIP Publishing*. [http://dx.doi.org/10.1063/1.4971178]

I. INTRODUCTION

The application of insulating metal oxides to high-mobility semiconductors (Ge and related SiGe, GeSn alloys, group $A_{III}B_V$ materials, etc.) usually results in interfaces with far more complex electronic structure than that of more conventional silicon/oxide systems.[1] This is primarily related to the exposure of the semiconductor surface to oxidant during insulator deposition, leading to the growth of a "native" oxide interlayer (IL). In contrast with the silicon case where a wide-bandgap SiO_2 IL is formed, oxidation of high-mobility semiconductors typically leads to compounds with a more narrow bandgap (In_2O_3, Ga_2O_3, GeO_x).[2] Furthermore, the oxides in the IL are often sub-stoichiometric and may host gap electron states that enable trap-assisted tunneling and effectively lower interface barriers. In some cases, even segregation of one element, e.g., arsenic,[3,4] at the interface is encountered as well as in-diffusion of semiconductor atoms (Ge, Sn, In) into the insulating oxide layer.[5,6] Evaluation of the effect these factors have on the interface barriers represents a significant experimental challenge because transport of charge carriers involves not only intrinsic band states of the semiconductor and insulator materials but also the IL-related contributions which are to be isolated against the background of intrinsic bands. In this work, we will demonstrate the possibility to solve this problem by means of photocurrent spectroscopy, enabling separation between the internal photoemission (IPE) and the displacement currents related to trap-related transitions at the semiconductor/insulator interface.

Besides dealing with the interface characterization methodology on the one side, the present study addresses interfaces of indium arsenide (InAs) with Al_2O_3, a subject of much interest by itself since in recent years, the InAs semiconductor has been proposed as a candidate material for a wide spectrum of electronic and optoelectronic devices. For example, atomic-layer deposition (ALD) of Al_2O_3 is suggested as forming a passivation layer that allows one to reduce the leakage current in InAs/GaSb super-lattice photodetectors.[7] Similarly, the InAs/Al_2O_3 stack can be used to improve the electrical quality of GaSb p-type channels.[8–10] Most importantly, InAs is considered as a high mobility electron channel in a variety of transistor configurations ranging from planar metal-oxide-semiconductor (MOS) field-effect transistors (FETs)[11–13] to nano-wire FETs[14,15] and band-to-band tunneling devices.[16,17]

The major difficulty in the realization of practically useful InAs-based transistors appears to be the poor electrical quality of interfaces with deposited oxide insulators. A high density of charge traps generally encountered at the InAs/oxide interfaces leads to degradation of electron mobility, increases the sub-threshold slope, enhances noise, etc.[18,19] Most of the effects correlate with electron trapping in the near-interface oxide layer(s) which brings up the above mentioned concern regarding the height of the energy barriers encountered by electrons at the interfaces of InAs with oxide insulators. In particular, the role of InAs oxidation during insulator deposition leading to the formation of an IL remains unclear, since the high diffusivity[6] of In can drastically modify the IL composition, e.g., making it very different from that found at earlier studied GaAs interfaces. Furthermore, diffusion of highly mobile In and its incorporation into the atomic matrix of the insulating oxide itself may significantly affect the electronic properties of the dielectric as suggested by observations of annealing-induced variations in the band alignment at the interfaces of $In_{0.53}Ga_{0.47}As$ with insulating Al_2O_3.[20]

Moreover, there is significant inconsistency between the InAs/Al_2O_3 band offsets reported in the literature: The results previously inferred from the heterojunction measurements, relying on the band offset transitivity hypothesis, suggest that the valence bands (VBs) of GaAs and InAs are energetically aligned, i.e., they follow the so-called common anion rule (cf. Fig. 1 in Ref. 21). However, the compilation based on the electron affinity values points to a ≈ 0.25 eV upshift of the VB top in $In_xGa_{1-x}As$ already for $x \approx 0.5$ (cf. Fig. 18 in Ref. 22). The latter prediction appears inconsistent with the IPE results, indicating that the energy barrier, Φ_e, between the VB top in $In_xGa_{1-x}As$ ($0 \leq x \leq 0.53$) alloys and the bottom of the oxide conduction band (CB) remains constant for the interfaces with HfO_2 ($\Phi_e = 3.35$ eV) and Al_2O_3 ($\Phi_e = 3.45$ eV),[23] in line with the results for the single-crystal (100)InAs/Al_2O_3 interfaces ($\Phi_e = 3.45$ eV, Ref. 24). However, a somewhat lower energy barrier between $In_xGa_{1-x}As$ VB and the bottom of the Al_2O_3 CB, $\Phi_e = 3.3$ eV, has been reported for $In_xGa_{1-x}As$ ($x = 0.53$ and $x = 0.75$), which is further reduced upon annealing.[20] In the case of interfaces between thin epitaxial $In_{0.53}Ga_{0.47}As$ and InAs layers with Al_2O_3, an even lower barrier of $\Phi_e = 3.2$ eV has been reported,[25] though a later analysis of the InAs/Al_2O_3 interfaces[26] affirms the value $\Phi_e = 3.45$ eV from Ref. 24. The exposed barrier variability points to the possible impact of indium oxidation and/or diffusion on the band alignment. For example, the slope of the Schottky plots of the electron barrier Φ_e shown in Refs. 26 and 27 would correspond to an unrealistically low value of the image force constant $\varepsilon_i < 1$ ($\varepsilon_i = 1$ in vacuum), indicating that the used assumption of an abrupt InAs/Al_2O_3 (or $In_{0.53}Ga_{0.47}As/Al_2O_3$) interface is inadequate.

In this work, we will present the systematic analysis of the IPE spectra at interfaces of single-crystal (100)InAs with amorphous (a-)Al_2O_3, leading to the demonstration that there are two different contributions to the photocurrent, i.e., band-to band and band-to-trap transitions. Besides providing a reliable determination of the intrinsic band alignment at the InAs/a-Al_2O_3 interface, the analysis indicates two significant effects, namely—the formation of an IL with an energy gap close to that of AlAs, and development of CB tail states in the a-Al_2O_3 layer which may be associated with in-diffusion of In during ALD of alumina. Eventually, the IL formation represents the critical factor impairing insulating properties of the oxide insulation.

II. EXPERIMENTAL

Since revealing the effect of the oxidation-grown IL on the band alignment at the InAs/a-Al_2O_3 interface represents one of the major goals of this study, we analyzed two types of samples fabricated by ALD of alumina [$Al(CH_3)_3$ (TMA) + H_2O, 250 °C, TMA pulse first] on the top of (100)-oriented single-crystal InAs wafers: One set of samples was prepared without removal of the native oxide prior to the ALD and another one subjected to native oxide removal (denoted as "pre-cleaned" samples). Using a buffered oxide etchant (BOE: 6 pts. 40% NH_4F +1 pt. 49% HF mixture), the latter was performed by 80 s etching in the 1:5 H_2O:BOE solution. The substrates used were (100)InAs single-crystals of n- and p-type conductivity with dopant concentrations of $\approx 4 \times 10^{17}$ and $\approx 2 \times 10^{17}$ cm^{-3}, respectively. The thickness of the insulating a-Al_2O_3 layers was 8 or 20 nm. For the sake of comparison, similar alumina layers were deposited by ALD on the top of imec-cleaned[28] (100) silicon wafers [p-type, boron doped with concentration $(0.5–1) \times 10^{15}$ cm^{-3}]. MOS capacitors were fabricated by deposition of semitransparent (13-nm thick) top metal (Au or Al) electrodes of 0.5 mm^2 area, and using a 0.5–μm thick Al blanket electrode as the backside contact. In both cases, the metallization was done by thermoresistive evaporation of the metal on an unheated substrate in high vacuum to avoid radiation damage of the sample.

The fabricated capacitors were used in IPE and photoconductivity (PC) experiments conducted at room temperature over the spectral range of 1.9–6.5 eV with a constant spectral resolution of 2 nm. As described earlier,[24,29] the quantum yield (Y) is defined as the photocurrent normalized to the incident photon flux. The spectral dependences of the yield were measured under different bias voltages applied to the top metal electrodes and then analyzed to find spectral thresholds of different charge injection processes. By comparing the photocurrent yield spectra measured in capacitors with different metal gate material and/or under different orientation of the electric field in the alumina layer, the injecting interface and, therefore, type of the photoinjected charge carrier can be identified.[30] As compared to the previous studies,[24,29] extensive signal averaging (>100 readouts) was applied to enable reliable detection of low-level displacement currents reaching a sensitivity in the 10^{-17} A range.

III. RESULTS AND DISCUSSION

Figure 1 shows an example of the photocurrent yield spectra corresponding to electron IPE from the InAs substrate (positive top Au metal bias) as measured on the

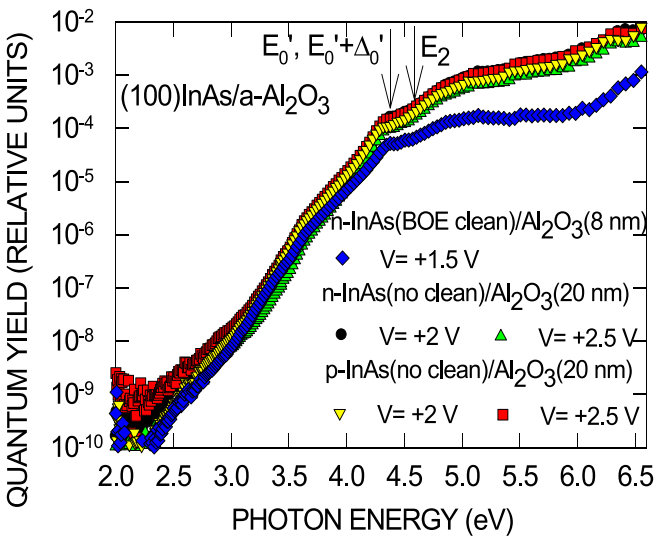

FIG. 1. Semi-logarithmic plot of the IPE quantum yield as a function of photon energy as measured on (100)InAs/a-Al_2O_3/Au samples prepared by using different InAs surface cleaning schemes. Vertical arrows E'_0, $E'_0+\Delta'_0$, and E_2 mark the energies of direct optical transitions in the InAs crystal.

samples prepared by ALD of alumina on InAs substrates with native oxide on top and on a substrate subjected to the BOE surface clean. Taking into account the built-in voltage drop of about 0.6–0.7 eV across the oxide caused by the work function difference between the Au electrode and the InAs substrate, the bias voltages applied for the spectra shown correspond to a strength of electric field close to 1 MV/cm in the alumina layer. This field is sufficiently large to saturate the quantum yield field dependence, i.e., no significant variation of the spectra can be seen over the applied changes in bias voltage. At the same time, the photocurrent in the spectral range above ≈4.5 eV is observed to decrease in the sample with the thinner oxide suggesting a contribution of optical transitions in the oxide bulk to the measured photocurrent. This observation brings to the fore importance of making separation between the electron photo-injection from the electrodes and the optical excitation of the oxide states. It will be discussed in more detail on the basis of additional measurements.

First, we address the spectral range below 4.5 eV in which the photocurrent spectra from the different samples exhibit similar behavior. Two features are observed in all spectral curves, i. e., at $h\nu = 4.4$ eV and 4.6 eV, marked by vertical arrows in Fig. 1, matching the known energies of optical singularities associated with excitation of direct transitions (E_0', $E_0'+\Delta_0'$) and E_2 in the InAs crystal,[31–33] respectively. This observation ensures that the photocurrent across the insulating alumina layer originates from the electron IPE from the InAs substrate. The absence of a substantial influence of the native oxide etching on the value of the quantum yield and its spectral distribution indicates that during ALD, the oxidized As and In compounds are effectively eliminated by the TMA—probably through a well known "self-cleaning" process.[34–36] Worth of adding here is that ALD of alumina on InP results in an IL with no Z-contrast in the transmission electron microscopy (TEM) images next to the Al_2O_3 overlayer, indicating the removal of In from the interface region through the oxide.[37]

However, if looking at lower photon energies, no optical features corresponding to E_1 and $E_1 + \Delta_1$ singularities in InAs can be seen in the spectral range $h\nu = 2.4$–2.8 eV which does suggest that the photocurrent generation mechanism at lower photon energies is unrelated to optical excitations of electrons in InAs. Rather, the featureless spectral curves in the range $h\nu = 2.0$–3.5 eV resemble the signals related to the excitation of electron states inside the IL between InAs and the oxide on top.[38] Therefore, the yield spectra shown in Fig. 1 apparently contain contributions stemming from at least two different photocurrent generation mechanisms.

The latter conclusion is supported by the analysis of the yield spectra measured under negative top metal bias on n- and p-type (100)InAs/Al_2O_3/Au samples as shown in panels (a) of Figs. 2 and 3, respectively. The reversal of the electric field splits the IPE spectra in two clearly distinctive parts: At $h\nu > 3.5$ eV, the photocurrent flow corresponds to the electron drift from the top metal electrode towards the InAs substrate and can be associated with the electron IPE from Au. However, at lower photon energies, a featureless spectrum of photocurrent of opposite direction is observed, with spectral

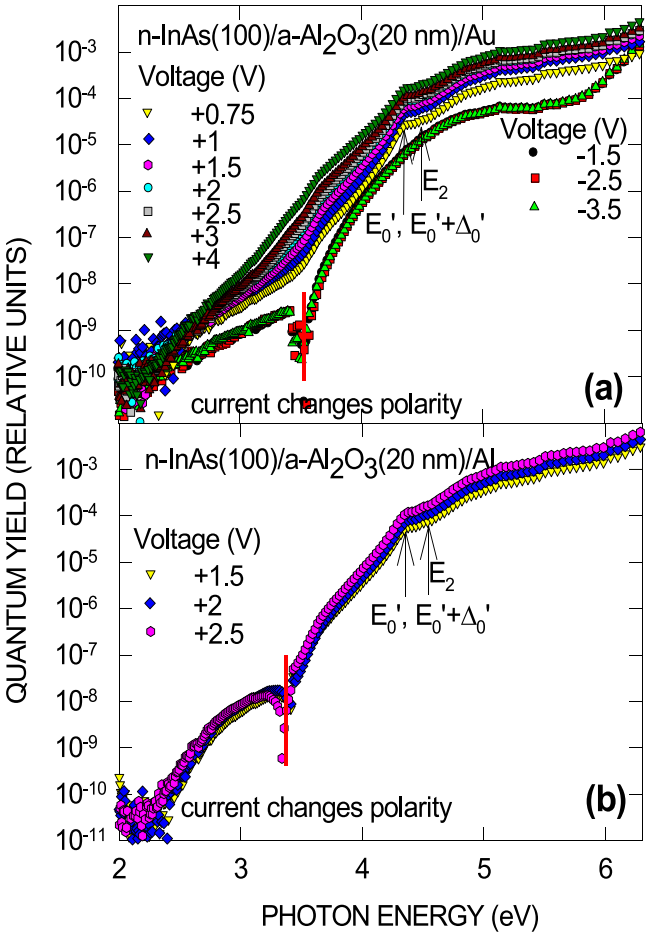

FIG. 2. Semi-logarithmic plot of the IPE quantum yield as a function of photon energy as measured on n-type (100)InAs/a-Al_2O_3 samples prepared on the un-etched InAs surface with Au (a) and Al (b) top metal electrodes. The voltages applied to the metal are indicated in the legend. Vertical arrows E'_0, $E'_0+\Delta'_0$, and E_2 mark the energies of direct optical transitions in the InAs crystal.

appearance closely resembling an attenuated version (≈10–20 times) of the signal seen in the same spectral range under positive bias (cf. Fig. 1). Obviously, electrons injected from InAs cannot drift across the Al_2O_3 layer against the electric field of repulsive polarity. Thus, the low-energy signal probably originates from a displacement current caused by recharging of traps in the insulator near the interface of InAs with Al_2O_3. Indeed, the ALD-grown alumina layers are known to contain a considerable density of electron traps (acceptor states)[39,40] which may trap electrons optically excited in the nearby electrode, thus leading to the observed low-level (<10 fA) re-charging current.

In order to verify the hypothesis regarding the trap-related current, photocurrent yield spectra were also measured on samples with Al metal electrodes instead of Au. The corresponding spectral curves are shown in panels (b) of Figs. 2 and 3 for the n- and p-type InAs/Al_2O_3/Al capacitors, respectively. As expected, due to the lower work function of Al compared to that of Au, the energy onset of electron IPE from the negatively biased top metal electrode is shifted to the lower photon energy, Φ_e(Al) [cf. Fowler plot shown in the inset in Fig. 3(b)]. But what is more revealing is that in the samples with Al metallization the low-energy photocurrent

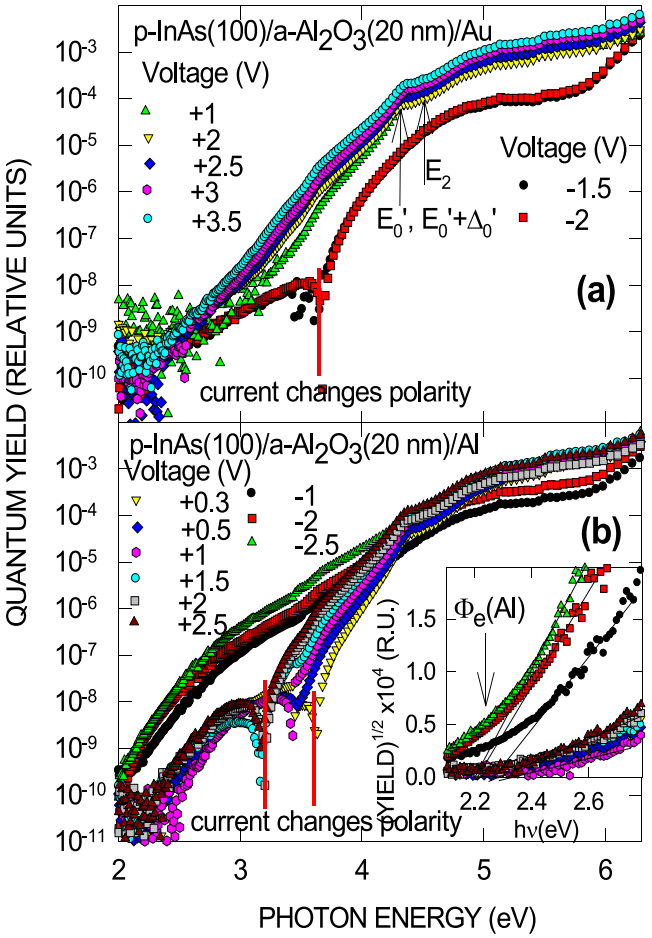

FIG. 3. Semi-logarithmic plot of the IPE quantum yield as a function of photon energy as measured on p-type (100)InAs/a-Al_2O_3 samples prepared on the un-etched InAs surface with Au (a) and Al (b) metal electrodes. The voltages applied to the metal are indicated in the legend. The vertical arrows E'_0, $E'_0+\Delta'_0$, and E_2 mark the energies of direct optical transitions in the InAs crystal. The inset in panel (b) illustrates the determination of the spectral threshold of electron IPE from Al into Al_2O_3 Φ_e(Al), using $Y^{1/2}$-hν (Fowler) plots.

[h$\nu < 3.5$ eV in Fig. 2(b)] measured under positive metal bias changes its direction to the opposite, corresponding to the electron motion from the Al gate towards the InAs substrate. This result allows us to associate this current with the capturing of electrons optically excited in the Al electrode by traps in the near-interface alumina layer. From the observed ratio between the photocurrent yield measured under negative bias and that observed under the reversed field orientation [$\approx 10^2$, cf. Fig. 2(b)], it becomes even possible to evaluate the average displacement of electrons in the direction opposite to the field as $\approx$1% of the alumina thickness, i.e., $\approx$0.2 nm. This length reflects the mean free path of an electron during its ballistic transport from Al into Al_2O_3. In turn, the optical excitation of electrons inside the IL between InAs and Al_2O_3 followed by their trapping in alumina would explain the low energy photocurrents in the Au-gated InAs/Al_2O_3/metal entities discussed in the previous paragraph.

An important result of the analysis of the Al-metallized samples consists in the clear separation between the spectral ranges corresponding to the trap-related displacement currents and to the signal caused by the electron IPE from InAs into Al_2O_3: As one can see from the spectra shown in panels (b) in Figs. 2 and 3 for the case of positive Al gate biasing, with increasing photon energy, the IPE current takes over the trap-related signal at h$\nu > 3.5$ eV, and therefore, this high-energy part of the IPE spectral curves can be used to reliably determine the IPE spectral threshold. This conclusion is independently supported by the observed stronger field dependence of the IPE threshold in the p-type InAs/Al_2O_3/Al sample [Fig. 3(b)] compared to the n-InAs case [Fig. 2(b)]. Indeed, this field effect is consistent with the apparent barrier lowering due to the penetration of the electric field into the depleted p-InAs layer,[24,30] causing an additional shift of the spectral threshold by a value comparable to the InAs bandgap width (0.36 eV at 300 K).

To find the spectral threshold of electron IPE from the VB of InAs, the yield spectra measured under positive metal bias were re-plotted using the Powell coordinates, $Y^{1/3}$-hν,[41] as illustrated in Fig. 4 for the n-type (100)InAs/a-Al_2O_3(20 nm)/Au sample. The observed abrupt increase of the yield above the level of the sub-threshold displacement current indicates the onset of electron photoemission from the InAs substrate. However, while for low bias voltages, one can easily find the spectral threshold, labeled as Φ_e(high) in Fig. 4, with increasing strength of the electric field in the alumina the threshold splits, suggesting the presence of an additional field-activated electron injection mechanism characterized by a somewhat lower energy threshold Φ^*_e(high).

In order to trace the physical origin of this barrier lowering, we conducted an additional experiment specifically focusing on photoemission of electrons from identically prepared (thermoresistive evaporation) Au and Al electrodes into the CB of 20-nm thick alumina layers ALD grown on p-InAs and the reference p-type Si substrates. Figure 5 shows examples of the corresponding spectra obtained under negative metal bias, facilitating electron injection from a metal, as the semi-logarithmic plots [panel (a)] or the Fowler ($Y^{1/2}$-hν) plots [panel (b)]. These spectra reveal a $\approx$0.3–0.4 eV electron

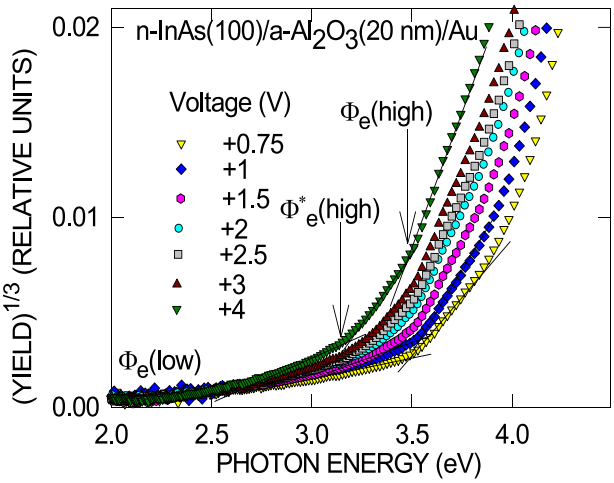

FIG. 4. Cube root of the IPE yield as a function of photon energy measured for different bias values applied to the n-type (100)InAs/a-Al_2O_3(20 nm)/Au capacitor, used to determine the spectral thresholds. The inferred thresholds Φ_e (low/high) of electron IPE from the VB of InAs into the CB of a-Al_2O_3 are indicated by arrows. Lines guide the eye.

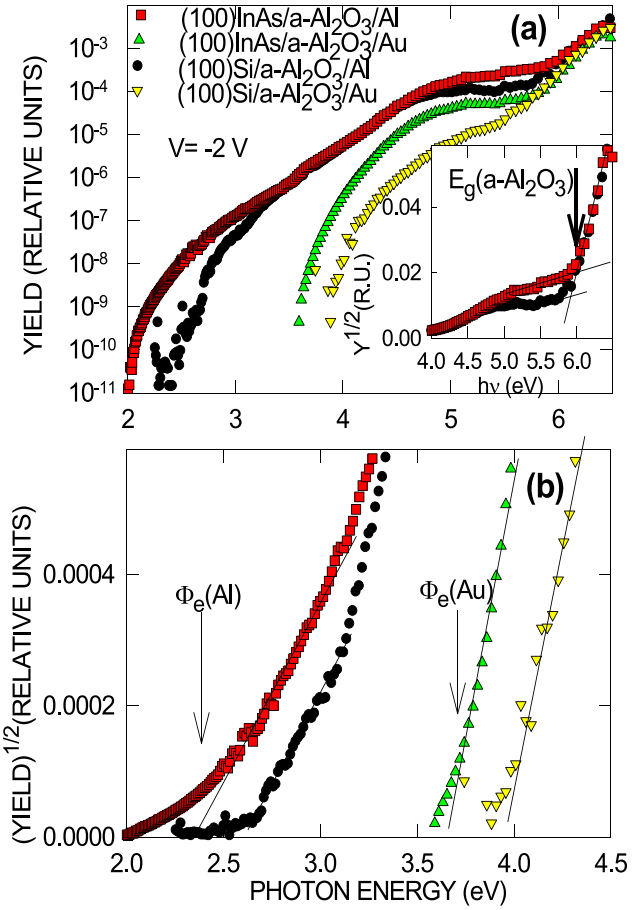

FIG. 5. Semi-logarithmic (a) and Fowler (b) plots of the IPE quantum yield as a function of photon energy measured on p-type (100)InAs/a-Al_2O_3 and (100)Si/a-Al_2O_3 samples with Au and Al top electrodes under −2 V bias voltage applied to the metal (electron IPE from the metal electrode into the CB of alumina). The vertical arrows mark the threshold energies of electron IPE from the metal into the alumina layer. The inset in panel (a) shows the $Y^{1/2}$-hν plot of the yield spectra in the photon energy range near the spectral threshold of the ALD alumina intrinsic photoconductivity. The vertical arrow marks the bandgap of the alumina layer E_g(a-Al_2O_3).

barrier lowering both at the Al/a–Al_2O_3 and Au/a-Al_2O_3 interfaces in the samples grown on p-(100)InAs substrates as compared to their counterparts fabricated on p-type (100)Si. Therefore, we conclude that a-Al_2O_3 films grown on InAs have low-energy CB "tail" states. We tentatively ascribe as a result from In in-diffusion, as discussed in the next paragraph. Apparently then, the barrier lowering observed at the InAs/a-Al_2O_3 interface is also due to modification of the oxide CB bottom part.

The inset in Fig. 5(a) compares the photocurrent yield spectra of 20-nm thick alumina layers grown by ALD on p-type InAs and Si substrates in the spectral range close to the onset of intrinsic PC of alumina E_g(a-Al_2O_3) ≈ 6 eV. The alumina layers grown by ALD on InAs exhibit an enhanced sub-threshold photoconductivity in the photon energy range $4.5 < h\nu < 6$ eV compared to the samples grown on Si. It is worth noting that the photocurrent in this spectral range is found to scale with the oxide thickness as discussed in relationship with the spectra shown in Fig. 1. This behavior can be correlated the in-diffusion of In from the interface into the oxide layer associated with reduction of native oxides.[35]

The effect of indium in-diffusion would also explain earlier observations regarding barrier height lowering caused by high-temperature annealing of samples prepared by ALD of Al_2O_3 on In-containing semiconductor substrates.[20] It would also agree with the later report regarding accumulation of In in the ALD-grown alumina layers on $In_{0.53}Ga_{0.47}As$.[42] Also, there is plentiful evidence of In transport across various insulating oxides ALD-grown on different In-containing substrates as revealed by several composition-sensitive techniques.[43–47] Therefore, our results concerning the impact of In on electronic properties of insulating Al_2O_3 may also be relevant to other In-containing material systems.

To determine the intrinsic (zero-field) barrier height between the InAs VB and the Al_2O_3 CB, the inferred IPE spectral thresholds, Φ_e(high), are plotted using the Schottky coordinates as illustrated in Fig. 6(a). Linear extrapolation to the zero field value yields the barrier heights found to be in the range of 3.45–3.50 eV, which coincide [within the accuracy of the measurements (0.05–0.1 eV)] with the earlier reported barriers at interfaces of GaAs and $In_xGa_{1-x}As$ ($x \leq 0.53$) alloys with ALD alumina grown on top.[23] In turn,

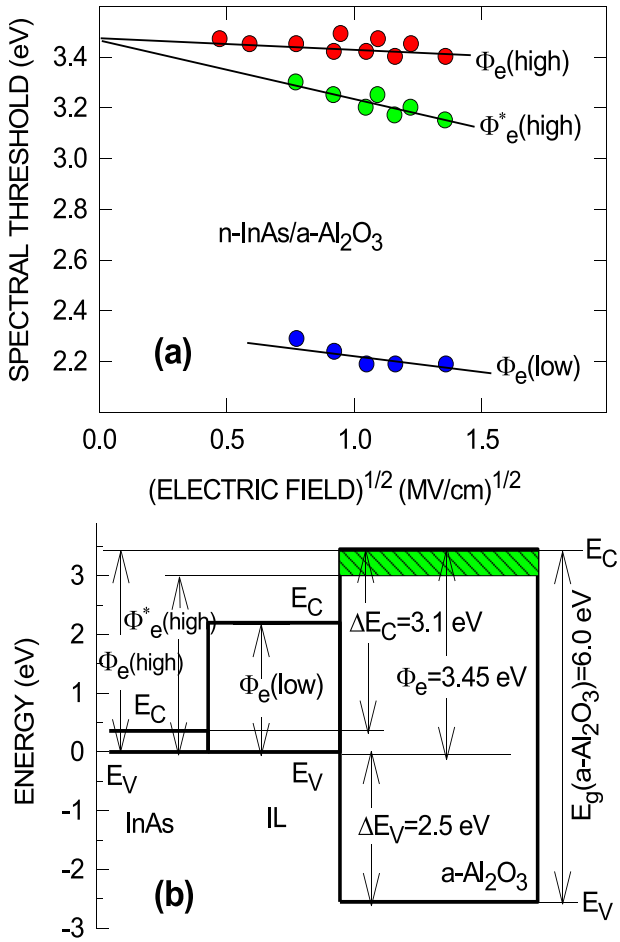

FIG. 6. (a) Determination of energy barrier at the InAs/a-Al_2O_3 interface using the Schottky plot of the IPE spectral thresholds; (b) schematic zero-field energy band diagram of the InAs/a–Al_2O_3 interface inferred from the current study. Top edges of the VB (E_V) and bottom edges of the CB (E_C) are indicated for InAs, IL, and a-Al_2O_3 as well as the measured electron barrier height Φ_e and the bandgap width of a-Al_2O_3 E_g(a-Al_2O_3). The inferred CB and VB offsets, ΔE_C and ΔE_V, are given for reference. The green dashed region schematically indicates the energy span of the CB-tail states.

the somewhat lower values of the barrier of 3.2–3.3 eV reported in the literature[20,25] can be explained by the electron photoinjection via the alumina CB tail states characterized by the lower threshold Φ^*_e(high). Therefore, we may conclude that replacement of Ga by In in arsenide semiconductors does not change the energy of the VB top, i.e., the bandgap narrowing from 1.42 eV in GaAs to 0.36 eV in InAs occurs predominantly by the shift of the CB bottom edge. The same energy of the VB top in the studied arsenides suggests the validity of the so-called common anion rule, which associates the VB states with common anions in the compounds—in the studied case, group V atoms.

For the sake of comparison, in Fig. 6(a) are also shown the values —falling in the range 2.1–2.3 eV— of the low-energy threshold Φ_e(low) inferred from the trap-related current spectra that are associated with electron excitation in the IL formed between InAs and a-Al_2O_3. It is worth noticing here that such spectral thresholds, in the 2.0–2.2 eV energy range, have also been reported in the literature for interfaces of different In-containing semiconductors, including not only InAs[25,26] but also $In_xGa_{1-x}As$,[20,27] with the ALD-grown alumina. The universal appearance of this threshold points to a similar origin of the electron states in these ILs. For example, the threshold at about 2.2 eV is very close to the bandgap width of AlAs (2.16 eV at 300 K). This observation may suggest that while In diffuses away from the interface region, the remaining As atoms interact with Al during the ALD of alumina. Indeed, on the basis of atomic analysis, it has even been suggested that bonding of As to Al may lead to the formation of a thin AlAs layer during ALD.[35] Though the available transmission electron microscopy (TEM) images[25,26] cannot directly support this hypothesis because of insufficient Z-contrast, the formation of Al-As bonds inside the IL and the corresponding electron states is well possible. It would then be logical to assign the low-energy ($h\nu < 3.5$ eV) portion of the photocurrent yield spectra to the optical excitation of AlAs-derived states in the IL followed by electron trapping in the near-interface alumina layer. One can roughly estimate the thickness of this narrow-gap IL from the ratio of the IL-related photocurrents observed at two opposite bias polarities (cf. Figs. 2 and 3), i.e., using the average displacement of photoexcited electrons as compared to the total oxide thickness. The obtained estimate of about 1 nm would agree with the width of the As distribution at the interface of InAs with an a-Al_2O_3 layer grown under similar conditions as reported in Ref. 15 (cf. Fig. 6).

Using this inference, the resulting InAs/Al_2O_3 interface band diagram can be schematically presented as shown in Fig. 6(b). If assuming that the upper edge of the occupied states in the AlAs IL is energetically also aligned with the top of the InAs VB, as it has been shown to be the case in GaAs, the IL in the current case will provide the energetically lowest barrier, of around 2 eV, for electron injection from the semiconductor VB into Al_2O_3. This hypothesis may also explain the earlier result on the determination of the tunneling barrier between these materials, revealing only ≈2.3-eV barrier,[11] which appears to be significantly lower than the ≈3.1 eV fundamental CB offset between InAs and Al_2O_3. Obviously then, tight control of the IL is needed to ensure a low electron injection rate from InAs into the insulating oxide, which may otherwise cause charge instability in the gate stack.

IV. CONCLUSIONS

Our results indicate that the "standard" model of an abrupt semiconductor/insulator transition cannot be used to adequately describe the spectrum of electron states at interfaces of single-crystal InAs with ALD-grown a-Al_2O_3 on top. Nevertheless, despite the more complex electron level structure, our photocurrent analysis has enabled the determination of the band alignment between InAs and a-Al_2O_3. The top of the InAs valence band is found at 3.45 ± 0.10 eV below the alumina CB bottom, corresponding to the CB and the VB offsets of 3.1 ± 0.1 eV and 2.5 ± 0.1 eV, respectively. These offsets are found to be insensitive to the BOE pre-deposition cleaning of the InAs surface and probably reflect intrinsic properties of the studied interface with no measurable interface dipole influence.

The analysis of IPE spectra reveals two additional factors contributing to the complexity of the picture: First, the out-diffusion of In and, possibly, its incorporation into the insulating oxide leads to the development of a ≈0.4 eV wide CB tail states band. At the same time, the top of the InAs VB measured relative to the alumina CB bottom remains at the same energy as in the earlier studied case of GaAs, thus supporting the validity of the "common anion" rule. Therefore, the bandgap narrowing in the $In_xGa_{1-x}As$ semiconducting alloys with increasing In content should predominantly occur through the shift of the CB bottom edge. Second, the interaction of the remaining As at the interface with Al during ALD apparently leads to the formation of an IL containing significant amount of Al–As bonds, which provide an additional low-barrier electron injection channel. The presence of this narrow-gap IL represents the major factor degrading the insulating properties of a-alumina ALD-grown on InAs.

ACKNOWLEDGMENTS

The work at KU Leuven was supported by the Fonds Wetenschappelijk Onderzoek—Vlaanderen (Project No. G.OCO5.13) and by Internal Fund Project No. C14/16/061. E.O'C. acknowledges the support from the grant "FACIT (Grant No. FP7-PEOPLE-2013-IEF-628523)." P.K.H. from Tyndall acknowledges the financial support of the European Commission through the project entitled "Compound Semiconductors for 3D Integration COMPOSE3" under Grant FP7-ICT-2013-11-619325.

[1]*Advanced Gate Stacks for High-Mobility Semiconductors*, edited by A. Dimoulas, E. Gusev, P. C. McIntyre, and M. Heyns (Springer, Berlin, 2007).
[2]V. V. Afanas'ev and A. Stesmans, in *Physics and Technology of High-k Gate Dielectrics–VII*, edited by S. Kar, M. Houssa, S. VanElshocht, and D. Landheer (Electrochemical Society, Pennington, NJ, 2009), pp. 95–103.
[3]M. Herrera, M. Chi, M. Bonds, N. D. Browning, J. N. Woolman, R. E. Kvaas, S. F. Harris, D. R. Rhiger, and C. J. Hill, Appl. Phys. Lett. **93**, 093106 (2008).
[4]F. S. Aguirre-Tostado, M. Milojevic, B. Lee, J. Kim, and R. M. Wallace, Appl. Phys. Lett. **93**, 172907 (2008).

[5]C. Merckling, X. Sun, Y. Shimura, A. Franquet, B. Vincent, S. Takeuchi, W. Vandervorst, O. Nakatsuka, S. Zaima, R. Loo, and M. Caymax, Appl. Phys. Lett. **98**, 192110 (2011).
[6]I. Krylov, R. Winter, D. Ritter, and M. Eizenberg, Appl. Phys. Lett. **104**, 243504 (2014).
[7]O. Salihoglu, J. Vac. Sci. Technol. B **32**, 051201 (2014).
[8]A. Greene, S. Madisetti, P. Nagaiah, M. Yakimov, V. Tokranov, R. Moore, and S. Oktyabrsky, Solid-State Electron. **78**, 56 (2012).
[9]A. Greene, S. Madisetti, M. Yakimov, V. Tokranov, and S. Oktyabrsky, Int. J. High Speed Electron. Syst. **23**, 1450015 (2014).
[10]M. Yokoyama, H. Yokoyama, M. Takenaka, and S. Takagi, Appl. Phys. Lett. **106**, 122902 (2015).
[11]N. Li, E. S. Harmon, J. Hyland, D. B. Salzman, T. P. Ma, Y. Xuan, and P. D. Ye, Appl. Phys. Lett. **92**, 143507 (2008).
[12]F. Xue, H. Zhao, Y.-T. Chen, Y. Wang, F. Zhou, and J. C. Lee, Appl. Phys. Lett. **98**, 082106 (2011).
[13]K. Takei, R. Kapadia, E. Pils, S. Krishna, and A. Javey, Appl. Phys. Lett. **102**, 153513 (2013).
[14]J. A. del Alamo, Nature **479**, 317 (2011).
[15]C. H. Wang, G. Doornbos, G. Astromskas, G. Vellianitis, R. Oxland, M. C. Holland, M. L. Huang, C. H. Lin, C. H. Hsieh, Y. S. Chang, T. L. Lee, Y. Y. Chen, P. Ramwall, E. Lind, W. C. Hsu, L. E. Wernersson, R. Droopad, M. Passlack, and C. H. Diaz, AIP Adv. **7**, 047108 (2014).
[16]M. Houssa, E. Chagarov, and A. Kummel, MRS Bull. **34**, 504 (2009).
[17]A. Seabough and Q. Zhang, Proc. IEEE **98**, 2095 (2010).
[18]G. Astromskas, K. Storm, and L.-E. Wernersson, Appl. Phys. Lett. **98**, 013501 (2011).
[19]K.-M. Persson, B. G. Malm, and L.-E. Wernersson, Appl. Phys. Lett. **103**, 033508 (2013).
[20]N. V. Nguyen, M. Xu, O. A. Kirillov, P. D. Ye, C. Wang, K. Cheung, and J. S. Suehle, Appl. Phys. Lett. **96**, 052107 (2010).
[21]S. Tiwari and D. J. Frank, Appl. Phys. Lett. **60**, 630 (1992).
[22]C. I. Hinkle, E. M. Vogel, P. D. Ye, and R. M. Wallace, Curr. Opin. Solid State Mater. Sci. **15**, 188 (2011).
[23]V. V. Afanas'ev, A. Stesmans, G. Brammertz, A. Delabie, S. Sionke, A. O'Mahony, I. M. Povey, M. E. Pemble, E. O'Connor, P. K. Hurley, and S. B. Newcomb, Appl. Phys. Lett. **94**, 202110 (2009).
[24]V. V. Afanas'ev, Adv. Condens. Matter Phys. **2014**, 301302.
[25]Q. Zhang, R. Li, R. Yan, T. Kosel, H. G. Xing, A. C. Seabaugh, K. Xu, O. A. Kirillov, D. J. Gundlach, C. A. Richter, and N. V. Nguyen, Appl. Phys. Lett. **102**, 012101 (2013).
[26]W. Li, Q. Zhang, R. Bijesh, O. A. Kirillov, Y. Liang, I. Levin, L.-M. Peng, C. A. Richter, X. Liang, S. Datta, D. J. Gundlach, and N. V. Nguyen, Appl. Phys. Lett. **105**, 213501 (2014).
[27]Q. Zhang, G. Zhou, H. G. Xing, A. C. Seabaugh, K. Xu, H. Sio, O. A. Kirillov, C. A. Richter, and N. V. Nguyen, Appl. Phys. Lett. **100**, 102104 (2012).
[28]M. Meuris, S. Verhaverbeke, P. W. Mertens, H. F. Schmidt, M. M. Heyns, M. Kubota, A. Philipossian, K. Dillenbeck, D. Graf, A. Schnegg, and R. de Blank, Microelectron. Eng. **22**, 21 (1993).
[29]V. V. Afanas'ev and A. Stesmans, J. Appl. Phys. **102**, 081301 (2007).
[30]V. V. Afanas'ev, *Internal Photoemission Spectroscopy* (Elsevier, Oxford, 2014).
[31]D. E. Aspnes and A. A. Studna, Phys. Rev. B **27**, 985 (1983).
[32]T. H. Ghong, T. J. Kim, J. W. Jung, Y. D. Kim, and D. E. Aspnes, J. Appl. Phys. **103**, 073502 (2008).
[33]T. J. Kim, J. J. Yoon, S. Y. Hwang, D. E. Aspnes, Y. D. Kim, H. J. Kim, Y. C. Chang, and J. D. Song, Appl. Phys. Lett. **95**, 111902 (2009).
[34]A. P. Kirk, M. Milojevic, J. Kim, and R. M. Wallace, Appl. Phys. Lett. **96**, 202905 (2010).
[35]R. Timm, A. Fian, M. Hjort, C. Thelander, E. Lind, J. N. Andersen, L.-E. Wernersson, and A. Mikkelsen, Appl. Phys. Lett. **97**, 132904 (2010).
[36]D. M. Zhernokletov, P. Laukkanen, H. Dong, R. V. Galatage, B. Brennan, M. Yakimov, V. Tokranov, J. Kim, S. Oktyabrsky, and R. M. Wallace, Appl. Phys. Lett. **102**, 211601 (2013).
[37]H.-Y. Chou, V. V. Afanas'ev, A. Stesmans, H. C. Lin, P. K. Hurley, and S. B. Newcomb, Appl. Phys. Lett. **97**, 132112 (2010).
[38]V. V. Afanas'ev, J. Appl. Phys. **113**, 166101 (2013).
[39]M. B. Zahid, D. R. Aguado, R. Degraeve, W. C. Wang, B. Govoreanu, M. Toledano-Luque, V. V. Afanas'ev, and J. Van Houdt, IEEE Trans. Electron Devices **57**, 2907 (2010).
[40]V. V. Afanas'ev, W. C. Wang, F. Cerbu, O. Madia, M. Houssa, and A. Stesmans, ECS Trans. **64**(8), 17 (2014).
[41]R. J. Powell, J. Appl. Phys. **41**, 2424 (1970).
[42]R. Winter, I. Krylov, C. Cytermann, K. Tang, J. Ahn, P. C. McIntyre, and M. Eizenberg, J. Appl. Phys. **118**, 055302 (2015).
[43]O. Ceballos-Sanchez, A. Sanchez-Martinez, M. O. Vasquez-Lepe, T. Duong, R. Arroyave, F. Espinosa-Magana, and A. Herrera-Gomez, J. Appl. Phys. **112**, 053527 (2012).
[44]W. Cabrera, B. Brennan, H. Dong, T. P. O'Regan, I. M. Povey, S. Monaghan, E. O'Connor, P. K. Hurley, R. M. Wallace, and Y. J. Chabal, Appl. Phys. Lett. **104**, 011601 (2014).
[45]O. Ceballos-Sanchez, E. Martinez, C. Guedj, M. Veillerot, and A. Herrera-Gomez, Appl. Phys. Lett. **106**, 221602 (2015).
[46]Y. Hu, C. Wang, H. Domg, R. M. Wallace, K. Cho, W.-H. Wang, and W. Wang, ACS Appl. Mater. Interfaces **8**, 7595 (2016).
[47]A. J. Henegar and T. Gougousi, J. Vac. Sci. Technol. A **34**, 031101 (2016).